LINAC ALIGNMENT TECHNIQUES[*]

W. B. Herrmannsfeldt
Stanford Linear Accelerator Center
Stanford University, Stanford, California

Summary

Techniques of aligning linear accelerators are discussed with specific reference to the alignment system of the two-mile accelerator. This system uses a "three-point" method by which a point which is to be aligned is brought into coincidence with the line as defined by its end points. The end points are a laser and a photo-electric detector. A rectangular Fresnel lens is located at each point to be aligned to define the "third point."

Introduction

The basic tolerance for the alignment of the Stanford two-mile accelerator is $\pm$ 0.5 mm over the total length of 3050 meters. This requirement is derived from the difference between the 16 mm aperture of the beam-scraping collimators and the smallest aperture in the 3-meter-long disk-loaded waveguide which is 18 mm. The difference of 2 mm can be divided evenly between the alignment and the functions of steering and focusing, thus leaving 1.0 mm, or $\pm$ 0.5 mm, for alignment.

Although the geological stability of the base of the accelerator housing is generally expected to be very good, estimates indicate that it may be necessary to check the alignment as frequently as once every one or two months. In order to prevent long shutdowns for surverying, the system is designed so that the alignment can be checked remotely while the accelerator is operating, without requiring personnel to enter the accelerator housing. Any indicated corrections to the alignment can then be planned in advance and made during a routine maintenance shutdown.

It is interesting to consider how two conventional alignment techniques would fare in view of the above requirements.

The method of optical tooling which involves aiming a telescope at a target is used for the alignment of the components on each of the 273 prefabricated segments from which the accelerator is assembled. The angular tolerances for the alignment of these segments, which range in length from 3 to 12 meters, is approximately 10^{-5} radians. While this accuracy is attainable, extending this method to the alignment of the entire accelerator would require that the telescope be aimed and held stable to within less than 10^{-7} radians (about 0.02 seconds of arc). This is impossible because of the vibrations from all the associated activities, including traffic on a nearby highway.

The conventional stretched wire technique has been used for alignment to similar tolerances over lengths of a few hundred meters at most. To extend it to 3050 meters, presumably by using overlapping segments, appears both uncertain and impractical in view of the requirement for remote survey.

The method which has been adopted for the final alignment system is illustrated in Fig. 1. A straight line is defined between a point source of light L and a detector D. The light source is a helium-neon laser. The detector consists of a mechanical scanning system and a photomultiplier with suitable output equipment capable of resolving a shift of 0.025 mm at any of the 274 support points. At each support point, a target T is supported on a remotely actuated hinge. Three additional targets are mounted on monuments, such as the one at M, which are 60-cm-diameter pillars supported by rock below the accelerator foundation. To check the alignment at a desired point, the target at that point is inserted into the light beam by actuating the hinge mechanism. The target is actually a rectangular Fresnel lens with the correct focal length so that an image of the light source is formed on the plane of the detector. This image is then scanned by the detector in both the vertical and the horizontal directions to determine the displacement of the target from the predetermined line.

The targets are mounted in a 60-cm-diameter aluminum pipe (see Fig. 2) which is the basic support girder for the accelerator. The support girder is evacuated to about 10 microns of Hg to prevent air refraction effects from distorting or deflecting the alignment image. If any adjustments are required, the support girder is moved by means of a pair of vertical screw jacks and a side wall screw jack.

The accelerator proper is mounted about 68 cm above the center of the support girder. Because the optical alignment system is only intended to align the support girder in the horizontal and vertical directions, it is necessary to provide an auxiliary system of levels to prevent azimuthal misalignment of the support girder which, to first order, would have the effect of horizontal misalignment of the accelerator. The azimuthal tolerance is about 1 minute of arc. Figure 3 is a photograph of an installed accelerator segment before the next preceding segment was moved in place.

Overall Description of the Alignment System

The accelerator is assembled from prefabricated segments which are approximately 12 meters long. The standard accelerator segment consists of four 3-meter-long sections of disk-loaded waveguide mounted on top of a 12-meter-long section of the 60-cm-diameter aluminum support girder. At the end of each sector, which consists of eight 12-meterlong segments, there is a special 3-meter-long drift section used for steering, focusing, and instrumentation. The standard drift section consists of focusing and steering magnets, beam monitoring devices and a 16-mm-diameter collimator mounted on a

3-meter-long segment of support pipe. There is a total of 30 such sectors, i.e., 240 of the 12-meter segments and 30 of the 3-meter drift sections, plus three extra segments for the injector and the positron source. As described above, each segment is supported at the input end by a pair of precision screw jacks from the floor and by a third jack from the wall, as shown in Fig. 2. The output end of a segment is attached to the beginning of the next segment by a pair of heavy guide pins which allow for thermal expansion. Both the support girders themselves and the four 3-meter-long accelerator sections supported on each of them are joined end-to-end by heliarc-welded bellows. A 7.5 cm aluminum end flange is welded to the input end of each segment of support pipe. The connecting pins from the three jacks are fastened to the outside of this flange. The target hinge assembly is mounted on the top of the inside surface of the flange. The accelerator sections are supported on adjustable brackets along the support pipe, except that the first support bracket for the section which begins above the flange is pinned in place. The whole design at the input flange is intended to provide the maximum rigidity for the support between the accelerator sections and the alignment target.

The alignment target is mounted on a 40-cm-square stainless steel frame. The hinged target support plate is spring-loaded to hold the target firmly against the lower stop when it is inserted in the light beam. A compressed air actuator holds the target horizontally against the top of the support girder when it is not being used. In this position the target is hidden behind a square baffle which is mounted in the output end of the adjacent segment of the support girder. One target at a time is to be inserted in the light beam produced by the laser. The target is inserted by operating the bellows actuator which is mounted in an opening on the top of the support girder. The control panel for the target actuator is in the two-mile-long klystron gallery located on the surface directly above the accelerator. Indicator lights wired to microswitches within the support girder show the position of the target to the operator in the klystron gallery. In addition, the operator of the detection equipment at the end of the accelerator has an indicator showing if any target in the entire system is not fully retracted. This indicator assures the operator that only one target at a time is affecting the pattern. The operator also has control switches to permit him to remotely insert one target at each drift section in order to make a quick survey of the key points along the accelerator.

A switching mirror system at the detector permits the operator to view the image on a ground glass or to direct it into either the vertical or the horizontal detection system.

The optical alignment system, as just described, is only as long as the accelerator; thus it does not aid in determining the location of slits, collimators, magnets and other components which comprise the Beam Switchyard (or "BSY"). Nor does it allow the alignment of equipment located in the experimental areas beyond the BSY. To aid in surveying the positions of the components in the BSY, an extension of the accelerator alignment system past the end of the accelerator has been provided. The extension consists of a 25-cm-diameter pipe tangent to the bottom of the 60-cm support girder. If all the accelerator targets are removed, the light beam can shine down the 25-cm pipe. The BSY system is tied to the accelerator alignment system by two double targets, one on the last monument, as described above, and one at the end of the accelerator. The upper pattern in the double targets is centered in the target frame just like any other target pattern. The lower pattern is positioned so that its image shines down the smaller extension pipe. The focal length of the Fresnel lens in the lower pattern is adjusted for the total length of the two systems combined.

In addition to the drift section targets, the operator at the detection station will also be able to control the three targets which are located on the reinforced concrete monuments supported on rock beneath the foundation of the accelerator. The monuments are isolated from the floor of the accelerator. The targets are supported in the evacuated pipe through bellows connections which permit the accelerator to be moved relative to the monument without moving the monument target. The last of the three monuments is located 5 meters ahead of the mirror at the end of the accelerator. One of the double targets for the BSY is mounted on this monument, and the other double target is mounted at the very last accelerator target position. Either of these targets, together with the laser point source, are the two points which determine the basic straight line for the alignment of the accelerator and the BSY.

The design of the precision screw jacks permits the optional installation of remote actuating devices. These actuators would permit an operator directly above the support point to make small alignment corrections without entering the accelerator housing. The complexity of the rf waveguides, which must move with the accelerator structure, and the distances involved rule out any attempt to construct a fully automatic alignment system. The remote actuators will initially be installed only at selected points where they are required.

The jacks are limited in travel to a range of $\pm$ 25 mm by incremental stops. In order to exceed this limit, a technician must enter the accelerator housing to change the stops. In principle, it is possible to move the accelerator by as much as $\pm$ 15 cm without hitting the walls of the housing. However, several complicated mechanical changes would have to occur before such a large adjustment could be made.

The alignment of the accelerator is dependent on keeping the support girder level in the transverse direction. Where remote jack actuators are used, it is also necessary to provide a means for remotely monitoring the transverse leveling. This is done with a remote-reading pendulum device. The

image pattern also provides an indication of azimuthal position. It will be shown below that the actual image pattern from the rectangular Fresnel lens is a cross with a bright center spot. The arms of the cross are intense enough to be used with the detector to determine azimuthal position. However, the sensitivity of the azimuthal determination is not sufficient over the entire length of the accelerator to enable the target pattern to be used throughout for this purpose. The loss of azimuthal sensitivity is due to the fact that while there is a magnification ratio of ℓ/r for all transverse displacements (see Fig. 1), there is no equivalent azimuthal magnification. The azimuthal sensitivity for the last two-thirds of the length of the accelerator is expected to be adequate because the resolution of the system only varies by a factor of three over that length.

Alignment System Components

The three basic elements of the alignment system are the light source, the target, and the detector. These are described below.

Light Source

The light source of the alignment system is a commercial He-Ne laser. The targets are designed for the fundamental visible wavelength of 6328 Angstroms. The laser is assembled using one spherical mirror and one plane mirror. The wavefront can be approximated by a spherical wave from a point source since the wave can be considered to emanate from a point whose size is determined by the diffraction-limited image of the illuminated part of the spherical mirror. Using Airy's law, the radius of the spot is 1.22 λ L/D, where L is the length of the laser, 60 cm, D is the diameter of the illuminated part of the spherical mirror, 0.6 cm, and λ = 6328 Angstroms. Thus the "point" is about 0.15 mm in diameter. The beam spreads to about 1.0% of the distance from the laser so that at 100 meters it would cover a spot 100 cm in diameter. To insure even illumination of the targets, especially the one closest to the laser, a diverging lens has been mounted in the laser beam. The lens does reduce the intensity of illumination of the targets, but it also greatly reduces the accuracy to which the laser must be pointed. The laser is designed to emit 1.0 mw of power which is expected to be sufficient for the detection system to operate with a signal-to-noise ratio well above the threshold for maximum sensitivity.

Alignment Targets

The targets are rectangular Fresnel-zone plates. The rectangular design is preferred over the classical circular zone plate primarily for reasons of fabrication. It is easier to rule straight lines than circles, and the circular zones would require special spiders for supports.

The one-dimensional Fresnel pattern is shown in Fig. 4. The distance from the center line of the target to the center of the nth slot is

$$X_n = (\lambda rs/2\ell)^{\frac{1}{2}} (4n)^{\frac{1}{2}} . \qquad (1)$$

This is the same expression that is derived for the radius of the 2n Fresnel zone in most standard optics texts.[1] In it, λ is the wavelength, r and s are respectively the distances from the target to the laser and to the detector, and $\ell = r + s$. The edges of the nth slot are at

$$X_{ni} = \left(\frac{\lambda rs}{2\ell}\right)^{\frac{1}{2}} (4n + C - 1)^{\frac{1}{2}}$$

and

$$X_{no} = \left(\frac{\lambda rs}{2\ell}\right)^{\frac{1}{2}} (4n + C + 1)^{\frac{1}{2}}. \qquad (2)$$

The subscripts "i" and "o" denote the inner and outer edges of a slot, respectively. The arbitrary constant C selects the point at which the slot edge will be located in each Fresnel zone. For example, the values 0.0 and 2.0 for C have the effect of making two patterns which are the inverse or negatives of each other.

The targets are formed by chemically milling the array of rectangular holes into a copper sheet which is about 35 cm square and 0.5 mm thick. The following step-by-step manufacturing process is used:

1. Rule the complete one-dimensional pattern on a coated glass plate with an automatic diamond-tipped ruling engine controlled by punched paper tape, generated from computer magnetic tape output.

2. Strip the coating from the area between the edges of the open slots to form the pattern shown in Fig. 4.

3. By a succession of photographic steps, all using contact printing, form a master pattern consisting of crossed images of the one-dimensional pattern as shown in Fig. 5.

4. Transfer the master pattern to the copper sheet by applying a light-sensitive coating known as photo-resist and by exposing the coated copper to the master pattern. The nature of the photo-resist coating is such that, after developing and fixing, it is possible to use a suitable solvent to wash away the coating where the copper has not been exposed. The resulting areas of clean copper may then be used for subsequent plating or etching operations.

5. Electroplate an 0.05-mm-thick layer of nickel on the clean copper to form the actual pattern of the target.

6. By chemical milling, remove the unplated copper to form the required pattern of holes as in Fig. 5. The chemical milling process is controlled to retain the copper behind the nickel plating wherever possible. Generally, some copper will remain if the width of the ribbon is greater than the thickness of the copper sheet.

7. Apply a thin flash-coating of nickel for protection to the target which now resembles the cross section view shown in Fig. 6.

8. Mount the target to the stainless steel frame by match drilling the target and the frame. The frame has a pair of holes which fit over

locating pins on the target hinge, thus completing the connection from the target to the accelerator.

Errors in the position of the edges of the apertures can always be divided into symmetric and asymmetric errors. The maximum error that can occur in finding the center of the target is essentially the magnitude of the asymmetric shift of the aperture edges. The tolerance for the aperture edges is 0.025 mm which is the same as the criteria for the sensitivity of alignment of each target.

Symmetric errors can only affect the intensity and sharpness of the image, never its position. The only important type of symmetric error is that which is proportional to the distance of the edge of the aperture from the center of the target. This error is equivalent to having the wrong focal length for the target as calculated from Eq. (2) where the focal length f is given by $f = rs/\ell$. The longitudinal distance by which each target can be moved without causing a reduction in alignment sensitivity greater than 10% has been calculated by a digital computer program. In many cases it was found possible to let one target pattern be used in two or more positions without exceeding the 10% limitation. In addition, it is frequently possible to use the same target at an exactly symmetrically located position relative to the center of the accelerator. This is equivalent to exchanging r and s in Eq. (2). As a result, a total of only 121 different patterns are required for the 274 target locations.

Most of the patterns are 30 cm square. However, a limit of 250 slots was set and, as a result, at the ends of the accelerator the targets have 250 lines in less than 30 cm. The smallest of the targets, which is the very last one, is only about 10 cm square. The smallest slot in this last target is about 0.1 mm wide. The target with the longest focal length, which is located at the center of the accelerator, has only 46 slots in each direction of the 30 cm square.

Detector

The spot or line width of the image at the detection station will vary from about 0.1 mm for the last target to about 10.0 mm for the target nearest the light source. Figure 7 shows a photograph of a typical image pattern. The point to be aligned is the spot at the intersection of the crossed lines. The most difficult targets to align will be the ones in the center of the accelerator. In this region, line widths are about 4.0 mm. The desired resolution of the alignment system is 0.025 mm. With a 2-to-1 enlargement ratio of a lens in the center of the accelerator, it is necessary to find the center of the spot to within 0.05 mm, or 1 part in 80 of the line width. This is better than a human operator could be expected to do routinely. Therefore an electronic scanning system has been devised which displays the derivative of the spot intensity as a function of detector position in the horizontal or vertical directions. Figure 8 shows the intensity curve of the central spot and the derivative of the intensity curve. The center of the spot is defined by the point where the

derivative is zero. The advantage of using this method is that the steep line intersecting the axis gives an unambiguous determination of the image center. Figure 9 shows the actual plots of the differentiated alignment image as obtained from an x-y recorder. Each curve was traced twice to establish the reproducibility of the results. The target was moved 0.1 mm between taking the two curves.

The second derivative of the peak, d^2I/dx^2, which is the slope of the line as it intersects the axis, is used as a measure of the sharpness of the image. When the second derivative of the intensity curve is multiplied by the peak intensity I_0, we obtain a measure of the error signal as a function of displacement of the image. When the square root of this quantity is multiplied by the magnification of the system, ℓ/r, the resulting product is proportional to the signal obtained by displacing the target, thus giving as a measure of the alignment sensitivity

$$\frac{d}{dx}(\text{output signal}) \propto \left[I_0\left(\frac{d^2I}{dx^2}\right)\right]^{\frac{1}{2}}_{x=0}\left(\frac{\ell}{r}\right). \quad (3)$$

Image Pattern

The calculation of the image intensity from a pattern of holes in a target plate involves the use of Fresnel integrals. Both Taylor series approximations of the integrals and digital computer programs have been used for calculating the expected images. The analytical approximations will be presented below for the rectangular Fresnel lens.

The intensity at the image plane of light which has passed through an arbitrary hole pattern is

$$I(P) = |U(P)|^2. \quad (4)$$

For a point source S, the amplitude U(P) is given by the Fresnel-Kirchoff diffraction integral which, to second order to the variables ξ and η describing the surface, is

$$U(P) = \frac{-Ae^{ik\ell}}{2\ell}\iint\limits_{target} e^{i\frac{\pi}{2}(\mu^2+\nu^2)}d\mu d\nu \quad (5)$$

where μ and ν are the normalized distances from the origin P on the target and are given by

$$\mu^2 = \frac{2\ell}{\lambda rs}\xi^2 \quad \text{and} \quad \nu^2 = \frac{2\ell}{\lambda rs}\eta^2. \quad (6)$$

The wave number is $k = 2\pi/\lambda$ and, as in Fig. 10, r and s are the target and image distances respectively and $\ell = r + s$. The source intensity is A^2 units-of-power/steradian.

By taking coordinates ξ and η parallel to the edges of the holes, we can separate the integrals in Eq. (5) and write

$$U(P) = \frac{-iAe^{ik\ell}}{2\ell} \int_\mu e^{i\frac{\pi}{2}\mu^2} d\mu \int_\nu e^{i\frac{\pi}{2}\nu^2} d\nu. \quad (7)$$

By substituting Eq. (7) back into Eq. (4), we have

$$I(P) = \left(\frac{A}{2\ell}\right)^2 \left\{ C^2\left[\mu(P)\right] + S^2\left[\mu(P)\right] \right\} \quad (8)$$

$$\left\{ C^2\left[\nu(P)\right] + S^2\left[\nu(P)\right] \right\} = \left(\frac{A}{2\ell}\right)^2 I_\mu I_\nu.$$

There are a variety of ways to design the target within the mechanical limitations. A simple illustration is to attempt to maximize the "C" integrals while minimizing the "S" integrals. If we write

$$C = \int \cos\left(\frac{\pi}{2}\mu^2 d\mu\right) \text{ and } S = \int \sin\left(\frac{\pi}{2}\mu^2\right)d\mu \quad (9)$$

and allow slots at $4n - 1 < \mu^2 < 4n + 1$ and ribbons at $4n + 1 < \mu^2 < 4n + 3$, the $\cos(\pi/2)\mu^2$ function will always be positive during intervals of contribution to the integral while the $\sin(\pi/2)\mu^2$ function will oscillate in a manner that causes the integral to be small. The nth slot will then have edges at

$$\xi_+ = \sqrt{\frac{\lambda rs}{2\ell}} \sqrt{4n + 1} \text{ and } \xi_- = \sqrt{\frac{\lambda rs}{2\ell}} \sqrt{4n-1}. \quad (10)$$

The addition of a constant C under the radical, as in Eq. (2), permits the arbitrary choice of phase such as we made in optimizing the cosine integrals. In the case of the targets for the main part of the accelerator, a support strip was required through the middle of each target. This prevented us from including the center or $n = 0$ slot. The best alternative was to make the central ribbon the same width (1 cm) in all targets. Since $\lambda f/2$ is different for each target, it is necessary to calculate C from the expression in Eq. (2) for the inner edge of the first slot, $X_{1-}^2 = (\lambda f/2) (3 + C)$, yielding

$$C = \frac{0.25}{(\lambda f/2)} - 3. \quad (11)$$

For this example we will continue to consider the case for $C = 0$, but without the center slot.

Having defined the target pattern as alternating slots and ribbons, we can rewrite the integrals as sums of integrals over the successive slots. Thus we can write

$$C(\epsilon) = \sum_{\substack{n=-N \\ n\neq 0}}^{N} \int_{\mu_{n-}(\epsilon)}^{\mu_{n+}(\epsilon)} \cos\left(\frac{\pi}{2}t^2\right) dt \quad (12)$$

and

$$S(\epsilon) = \sum_{\substack{n=-N \\ n\neq 0}}^{N} \int_{\mu_{n-}(\epsilon)}^{\mu_{n+}(\epsilon)} \sin\left(\frac{\pi}{2}t^2\right) dt, \quad (13)$$

where ϵ is the normalized displacement from P at the point where the line from L to the point of interest on the image plance crosses the target. Thus for the intensity at the peak, the integrals are evaluated for $\epsilon = 0$. By measuring ϵ in the normalized coordinates, as in Eq. (6), the slot edges, which are the limits of integration, become

$$\mu_{n-}(\epsilon) = \sqrt{4n-1} - \epsilon \text{ and } \mu_{n+}(\epsilon) = \sqrt{4n+1} - \epsilon$$

for $n > 0$ and $\quad (14)$

$$\mu_{n-}(\epsilon) = -\sqrt{4|n|+1} - \epsilon \text{ and } \mu_{n+}(\epsilon) = -\sqrt{4|n|-1} - \epsilon,$$

for $n < 0$.

To analyze the intensity of the image near the central maximum we express the one-dimensional intensity of Eq. (8) as a power series in ϵ. Thus we have

$$I_\mu(\epsilon) = C^2(0) + S^2(0) + \epsilon\left[2C\frac{\partial C}{\partial\epsilon} + 2S\frac{\partial S}{\partial\epsilon}\right]_{\epsilon=0}$$
$$+ \frac{\epsilon^2}{2}\left[2\left(\frac{\partial C}{\partial\epsilon}\right)^2 + 2C\frac{\partial^2 C}{\partial\epsilon^2} + 2\left(\frac{\partial S}{\partial\epsilon}\right)^2 + 2S\frac{\partial^2 S}{\partial\epsilon^2}\right]_{\epsilon=0} + \cdots \quad (15)$$

where

$$\frac{\partial C}{\partial\epsilon} = -\sum_n \left[\cos\left(\frac{\pi}{2}\mu_{n+}^2\right) - \cos\left(\frac{\pi}{2}\mu_{n-}^2\right)\right],$$

$$\frac{\partial^2 C}{\partial\epsilon^2} = -\pi\sum_n \left[\mu_{n+}\sin\left(\frac{\pi}{2}\mu_{n+}^2\right) - \mu_{n-}\sin\left(\frac{\pi}{2}\mu_{n-}^2\right)\right],$$

$$\frac{\partial S}{\partial\epsilon} = -\sum_n \left[\sin\left(\frac{\pi}{2}\mu_{n+}^2\right) - \sin\left(\frac{\pi}{2}\mu_{n-}^2\right)\right], \text{ and}$$

$$\frac{\partial^2 S}{\partial\epsilon^2} = \pi\sum_n \left[\mu_{n+}\cos\left(\frac{\pi}{2}\mu_{n+}^2\right) - \mu_{n-}\cos\left(\frac{\pi}{2}\mu_{n-}^2\right)\right].$$

For the range of boundaries of interest, good approximations for the integrals are[2]

$$\int_0^\mu \cos\left(\frac{\pi}{2}t^2\right) dt \approx \frac{1}{2} - \frac{1}{\pi\mu}\left[\frac{\cos\left(\frac{\pi}{2}\mu^2\right)}{\pi\mu^2} - \sin\left(\frac{\pi}{2}\mu^2\right)\right] \quad (16)$$

and

$$\int_0^\mu \sin\left(\frac{\pi}{2}t^2\right) dt \approx \frac{1}{2} - \frac{1}{\pi\mu}\left[\frac{\sin\left(\frac{\pi}{2}\mu^2\right)}{\pi\mu^2} - \cos\left(\frac{\pi}{2}\mu^2\right)\right]. \quad (17)$$

Using Eq. (16), we have

$$C(0) = \sum_1^N \int_{\mu_{n-}}^{\mu_{n+}} \cos\left(\frac{\pi}{2}\, t^2\right) dt + \sum_{-1}^{-N} \int_{\mu_{n-}}^{\mu_{n+}} \cos\left(\frac{\pi}{2}\, t^2\right) dt$$

$$= \frac{1}{\pi}\left[\sum_1^N \left\{\frac{\pi}{2} - \frac{\cos\left(\frac{\pi}{2}\right)\mu^2}{\pi\mu^3} + \frac{\sin\left(\frac{\pi}{2}\right)\mu^2}{\mu}\right\}_{(4n-1)^{\frac{1}{2}}}^{(4n+1)^{\frac{1}{2}}}\right.$$

$$\left. + \sum_{-1}^{-N} \left\{\frac{\pi}{2} - \frac{\cos\left(\frac{\pi}{2}\mu^2\right)}{\pi\mu^3} + \frac{\sin\left(\frac{\pi}{2}\mu^2\right)}{\mu}\right\}_{-(4|n|+1)^{\frac{1}{2}}}^{-(4|n|-1)^{\frac{1}{2}}}\right]$$

$$= \frac{2}{\pi}\sum_1^N\left[(4n+1)^{-\frac{1}{2}} + (4n-1)^{-\frac{1}{2}}\right] \approx \frac{2}{\pi}\sum_1^N n^{-\frac{1}{2}}. \quad (18)$$

Similarly, we can show that

$$S(0) \approx -\frac{2}{\pi^2}\sum_1^N\left[(4n+1)^{-\frac{3}{2}} + (4n-1)^{-\frac{3}{2}}\right] \approx \frac{-1}{2\pi^2}\sum_1^N n^{-\frac{3}{2}}. \quad (19)$$

Except for small values of N, the contribution of $S^2(0)$ to $I_\mu(0)$ is negligible. The sum for $C(0)$ can be approximated by

$$\sum_1^N n^{-\frac{1}{2}} \approx \frac{1}{2}\left[\int_2^{N+1} n^{-\frac{1}{2}}\, dn + \int_2^{N+1}(n-1)^{-\frac{1}{2}}\, dn\right] + 1 \tag{20}$$

$$= (N+1)^{\frac{1}{2}} + N^{\frac{1}{2}} - 2^{\frac{1}{2}}.$$

Thus we have

$$C^2(0) = \frac{4}{\pi^2}\left[(N+1)^{\frac{1}{2}} + N^{\frac{1}{2}} - 2^{\frac{1}{2}}\right]^2 \tag{21}$$

which agrees with computer calculations of $I(0)$ within $\frac{1}{4}\%$ for $N > 25$.

In completing the expansion to second order for Eq. (15), we find, using the above method,

$$\left.\frac{\partial C}{\partial\epsilon}\right|_0 = \left.\frac{\partial S}{\partial\epsilon}\right|_0 = \left.\frac{\partial^2 S}{\partial\epsilon^2}\right|_0 = 0. \tag{22}$$

The only non-zero term for second order is

$$\frac{\partial^2 C}{\partial\epsilon^2} = -2\pi\sum_1^N\left[(4n+1)^{\frac{1}{2}} + (4n-1)^{\frac{1}{2}}\right] \approx -8\pi\sum_1^N n^{\frac{1}{2}}$$

$$\approx -4\pi\left[\int_1^{N+1} n^{\frac{1}{2}}\, dn + \int_1^{N+1}(n-1)^{\frac{1}{2}}\, dn\right]$$

$$= -\frac{8\pi}{3}\left[(N+1)^{\frac{3}{2}} + N^{\frac{3}{2}} - 1\right]. \tag{23}$$

Substituting Eqs. (21), (22), and (23) into Eq. (15) we have

$$I_\mu(\epsilon) \approx \frac{4}{\pi^2}\left[(N+1)^{\frac{1}{2}} + N^{\frac{1}{2}} - 2^{\frac{1}{2}}\right]^2 \tag{24}$$

$$\left[1 - \epsilon^2 \frac{4\pi^2}{3}\frac{(N+1)^{\frac{3}{2}} + N^{\frac{3}{2}} - 1}{(N+1)^{\frac{1}{2}} + N^{\frac{1}{2}} - 2^{\frac{1}{2}}} + \cdots\right]$$

For an alignment target formed by superimposing identical patterns at right angles to each other, we can use

$$I_\mu(0) = I_\nu(0) \tag{25}$$

Then, from Eq. (8), with $N \gg 1$, we have

$$I(\epsilon) = \left(\frac{A}{\ell}\right)^2 \frac{64N^2}{\pi^4}\left[1 - \epsilon^2 \frac{4\pi^2 N}{3} + \cdots\right] \tag{26}$$

which describes the intensity near the peak along one of the axis lines through the center, as in Fig. 7.

Vacuum System

The light pipe must be evacuated to eliminate refractive effects due to the air. At a pressure of 1000 microns the curvature of the light beam due to the pressure gradient induced by gravity becomes negligible. However, reasonable estimates of the temperature gradient from top to bottom of the light pipe are such that the pressure must be reduced to about 10 microns to eliminate curvature due to the temperature gradient in the residual gas. A large pumping system is located at one end of the light pipe. It should be capable of evacuating the entire light pipe to 10 microns or less in 16 hours.

Detector Signals

The methods used to analyze the image intensity from the rectangular Fresnel lens will not be extended to study the signal from the detector. The image is scanned in one direction at a time by a linearly oscillating aperture which moves parallel to the direction in which the scanning motion is made. A phase-sensitive detector is used to analyze

the signal. To get an analytical conception of the signal amplitude, slope, and line width, we will expand the image in a Taylor series.

If $H(x,y)$ describes an aperture located at x and y on the image plane, the power into a photomultiplier tube placed behind the aperture is

$$P(x,y) = \left(\frac{A}{2\ell}\right)^2 \int\limits_{H(x,y)} I(\xi)\, I(\eta)\, d\xi d\eta \ . \qquad (27)$$

As defined in Eq. (6), ξ and η are measured in the target plane. $I(\xi)$ and $I(\eta)$ can be expanded in a Taylor series as

$$I(\xi) = I(0) + I^{(1)} + \frac{\xi^2}{2} I^{(2)} + \dots \qquad (28)$$

where $I^{(n)} = \dfrac{\partial^n I}{\partial \xi^n}\bigg|_{\xi=0}$

It is convenient to calculate using a rectangular aperture with dimensions 2a wide by 2b high. Then the integral in Eq. (27) becomes

$$\int\limits_{H(x,y)} I(\xi)\, I(\eta)\, d\xi d\eta = \left(\frac{r}{\ell}\right)^2 \int\limits_{x-a}^{x+a} I(\xi)\, d\xi \int\limits_{y-b}^{y+b} I(\eta)\, d\eta \qquad (29)$$

where the r/ℓ factors come from measuring ξ and η at the image plane.

If the scan is made in the x-direction right through the peak of the image at $y = 0$, we have

$$\frac{r}{\ell} \int\limits_{-b}^{b} I(\eta)\, d\eta = 2I(0)b + \frac{2}{3!} I^{(2)}b^3 + \dots = G(0) \qquad (30)$$

and

$$\frac{r}{\ell} \int\limits_{x-a}^{x+a} I(\xi)\, d\xi = 2I(0)a + \frac{1}{2}\left[(x+a)^2 - (x-a)^2\right] I^{(1)}$$
$$+ \frac{1}{3!}\left[(x+a)^3 - (x-a)^3\right] I^{(2)}$$
$$+ \frac{1}{4!}\left[(x+a)^4 - (x-a)^4\right] I^{(3)}$$
$$+ \frac{1}{5!}\left[(x+a)^5 - (x-a)^5\right] I^{(4)}$$
$$+ \dots$$
$$= 2I(0)a + 2xaI^{(1)} + \left(ax^2 + \frac{a^3}{3}\right) I^{(2)}$$
$$+ \frac{xa}{3}\left(x^2 + a^2\right) I^{(3)}$$
$$+ \frac{2a}{5!}\left(5x^4 + 10x^2a^2 + a^4\right) + \dots$$
$$= F(x) \qquad (31)$$

The motion of the aperture is described by

$$x = x_0 + d \sin wt \qquad (32)$$

where x_0 is the position of the center of oscillation at time t and the amplitude of oscillation is d. From Eq. (32) we have

$$x^2 = x_0^2 + 2x_0 d \sin wt + d^2 \sin^2 wt,$$
$$x^3 = x_0^3 + 3x_0^2 d \sin wt + 3x_0 d^2 \sin^2 wt + d^3 \sin^3 wt, \text{ and}$$
$$x^4 = x_0^4 + 4x_0^3 d \sin wt + 6x_0^2 d^2 \sin^2 wt + 4x_0 d^3 \sin^3 wt$$
$$+ d^4 \sin^4 wt \qquad (33)$$

The output signal can be obtained in terms of the primary oscillating frequency and harmonics by using the following standard trigonometric identities:

$$\sin^2 wt = \frac{1}{2} - \frac{1}{2}\cos 2wt,$$
$$\sin^3 wt = \frac{3}{4}\sin wt - \frac{1}{4}\sin 3wt, \text{ and}$$
$$\sin^4 wt = \frac{3}{8} - \frac{1}{2}\cos 2wt + \frac{1}{8}\cos 4wt. \qquad (34)$$

The Fourier analysis can then be made by combining Eqs. (31) through (34) and grouping terms with the same harmonic number. When this is done, the terms with the fundamental frequency are

$$\frac{\ell}{r} F_1(x_0) = 2I^{(1)}ad + 2I^{(2)}adx_0 + I^{(3)}a\left[x_0^2 d + \frac{a^2 d}{3} + \frac{d^3}{4}\right]$$
$$+ \frac{1}{3} I^{(4)}a\left[x_0^3 d + \frac{3}{4}x_0 d^3 + x_0 a^2 d\right] + \dots \qquad (35)$$

To evaluate Eq. (35) we use the result that (by comparing Eqs. (21) and (24)

$$I_\mu(\epsilon) \approx \left[\sum_{\substack{n=-N \\ n \neq 0}}^{N} \int_{\mu_{n-}(\epsilon)}^{\mu_{n+}(\epsilon)} \cos\left(\frac{\pi}{2}t^2\right) dt\right]^2 = C^2(\epsilon). \qquad (36)$$

From the definition in Eq. (6) we have, from Eq.(28)

$$\frac{r}{\ell} I^{(n)} = \left(\frac{2r}{\lambda \ell s}\right)^{\frac{n}{2}} \frac{\partial^n I_\mu}{\partial \epsilon^n} \qquad (37)$$

where the derivatives are found by successive differentiation of Eq. (36).

The derivatives of the $C(\epsilon)$ integrals follow the pattern used after Eq. (15). If we use the same model target that was assumed in the analysis of the rectangular Fresnel lens the limits of integration are the same as given by Eq. (14).

Predictably, we find that the odd derivatives are

$$\frac{\partial C}{\partial \epsilon}\bigg|_{\epsilon=0} = \frac{\partial^3 C}{\partial \epsilon^3} = 0 \ . \qquad (38)$$

For the even derivatives; $C(0)$ and $\partial^2 C/\partial \epsilon^2\big|_{\epsilon=0}$ are given by Eqs. (21) and (23), respectively. Continuing to the forth derivative from Eq. (15), we obtain,

$$\frac{\partial^4 c}{\partial \epsilon^4} = \frac{32}{5} \pi^3 \left[(N+1)^{5/2} + N^{5/2} - 1 \right]. \quad (39)$$

Combining Eqs. (35) through (39), we find the coefficient of the fundamental frequency is

$$F_1(x_o) \approx - \frac{2r}{\lambda\ell s} (2adx_o) \frac{128N^2}{3} \left[1 - \left(\frac{2r}{\lambda\ell s}\right) \left(x_o^2 \right.\right.$$

$$\left.\left. + \frac{3}{4} d^2 + a^2 \right) \frac{16\pi^2 N}{15} + \cdots \right]. \quad (40)$$

The width of the image can be defined as the distance between maximum and minimum of $F_1(x_o)$. As such, it is approximately the distance between the positive and negative peaks in Figs. 8 and 9, and is about equal to the full width at half maximum. If we assume a and d are small compared to the distance to the maximum or minimum, x_m, we have

$$1 - \frac{16\pi^2}{5} N x_m^2 \left(\frac{2r}{\lambda\ell s}\right) = 0, \text{ by setting } \frac{dF_1(x_o)}{dx_c} = 0.$$

From this we find

$$x_m = \pm \left[\frac{16\pi^2}{5} N \frac{2r}{\lambda\ell s} \right]^{-\frac{1}{2}}. \quad (41)$$

Thus the line width, $x_{max} - x_{min}$, is proportional to $(Nr/s)^{-\frac{1}{2}}$.

In practice the light pipe is a constant diameter, thus limiting the targets to a fixed maximum width. If we let $\mu^2 = 4N$ in Eq. (6), ξ would equal the half width of a target so that the effective width of a target is

$$D = \left(\frac{8N\lambda rs}{\ell}\right)^{\frac{1}{2}}. \quad (42)$$

Combining Eqs. (41) and (42), the width of the image is found to be

$$W \approx \sqrt{5} \left(\frac{\lambda s}{\pi D}\right) \quad (43)$$

which, in the middle of the accelerator, is 4.5 mm.

The detection sensitivity is equal to the derivative of the first harmonic coefficient at $x_o = 0$. Combining Eqs. (27) and (30) and differentiating, we have

$$\left.\frac{dP_1}{dx}\right|_{x_o=0} \approx \left(\frac{A}{2\ell}\right)^2 G(0) \left.\frac{dF_1}{dx_o}\right|_{x_o=0}$$

which, when we substitute from Eqs. (30) and (40) is

$$\left.\frac{dP_1}{dx}\right|_{x_o=0} \approx - \left(\frac{A}{2\ell}\right)^2 \left(\frac{16N}{\pi^2} 2b\right) \left(\frac{2r}{\lambda\ell s}\right) \left(\frac{256N^2}{3} ad\right). \quad (44)$$

If we let the dimensions of the aperture be proportional to the image width such that $b = 2a = fw$, where f is a constant of proportionality, Eq. (44) reduces to

$$\left.\frac{dP_1}{dx}\right|_{x_o=0} \approx -17 \left(\frac{A}{2\ell}\right)^2 N^2 f^2 d. \quad (45)$$

With a laser source that emits 1 mw into a solid angle of $4\pi \times 10^{-4}$ steradians, $(A/2\ell)^2 \approx 2 \times 10^{-12}$ watts/cm² for $\ell \approx 3 \times 10^5$ cm. If we assume the sweep amplitude d of the scanner is equal to w/2, we find

$$\left|\frac{dP_1}{dx}\right| \approx 1.7 \times 10^{-11} N^2 f^2 w \text{ watts/cm}.$$

In the center of the accelerator the targets only have 46 lines, or N = 23. If we let f = 1/10, $|dP_1/dx| \approx 4 \times 10^{-10}$ watts/cm. However, since the image from the center target moves twice as far as the target, the alignment sensitivity is

$$\left|\frac{dP_1}{d\xi}\right| = \frac{\ell}{r} \left|\frac{dP_1}{dx}\right| \quad (46)$$

which for the center target is about 8×10^{-10} watts/cm. To detect a shift of 0.025 mm in the target requires a differentiation of

$$\frac{\ell}{r} \left|\frac{dP_1}{dx}\right| \approx 4 \times 10^{-14} N^2 f^2 w\ell/r \text{ watts} \quad (47)$$

or 10^{-12} watts for the middle target. The peak intensity, which is the energy striking the photomultiplier at the center of the image, is, from Eqs. (26) and (30),

$$I(0) = \left(\frac{A}{2\ell}\right)^2 \left(\frac{256N^2}{\pi^4}\right)(2b)(2a) = \left(\frac{A}{2\ell}\right)^2 \frac{512N^2}{\pi^4} f^2 w^2 \text{ watts.} \quad (48)$$

At the center of the accelerator this is about 8.5×10^{-12} watts.

List of References

1. E.g., F. Jenkins and H. White, Fundamentals of Optics, 3rd edition (McGraw)-Hill, New York, 1957).

2. M. Born and E. Wolf, Principles of Optics (Macmillan, New York, 1964).

L - LASER
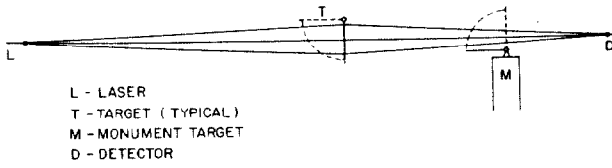T - TARGET (TYPICAL)
M - MONUMENT TARGET
D - DETECTOR

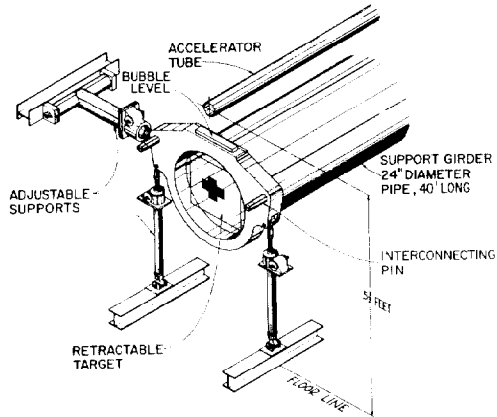Fig. 1. The alignment system, schematic diagram.

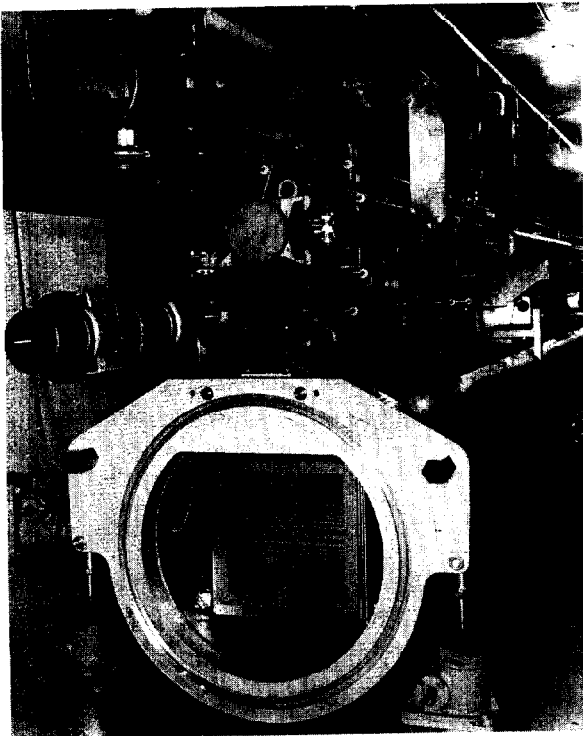Fig. 2. Accelerator support system.

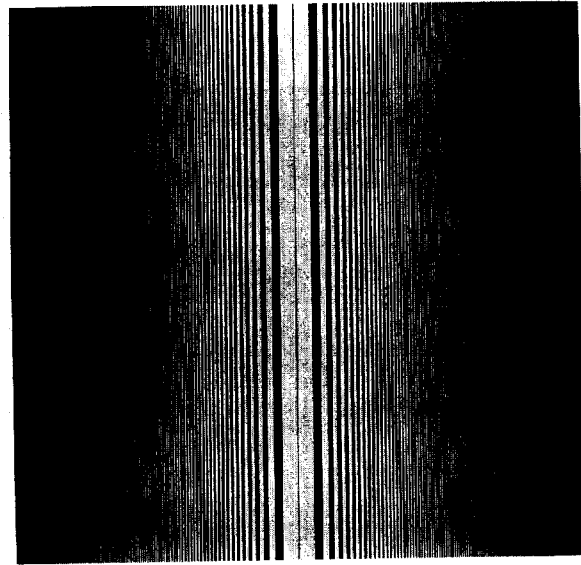Fig. 3. Installed segment of accelerator.

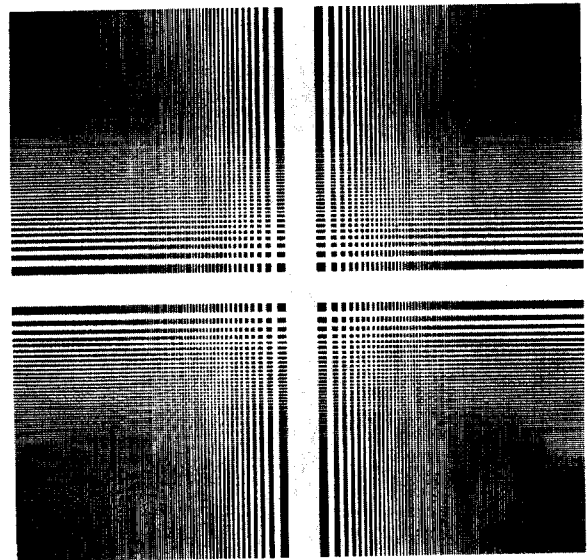Fig. 4. One-dimensional Fresnel zone pattern.

Fig. 5. Complete rectangular Fresnel pattern.

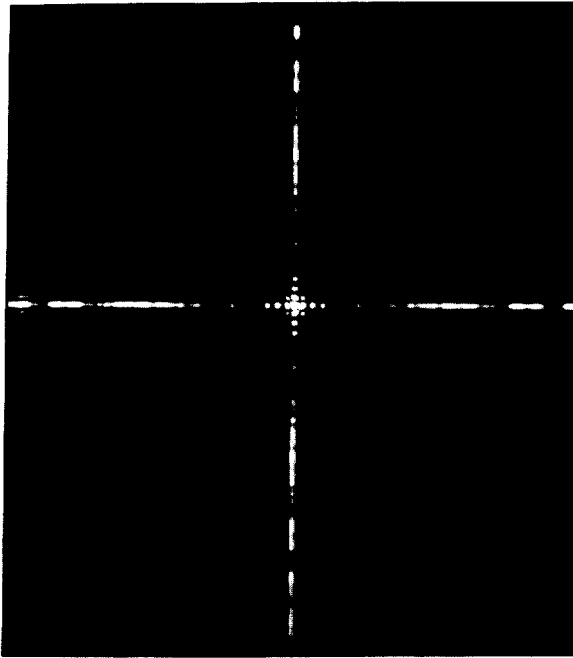Fig. 6. Cross section of target showing edges of aperture.
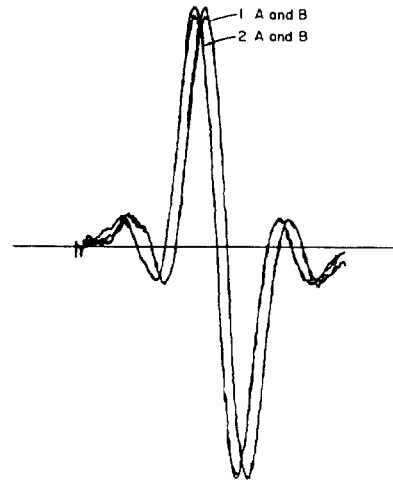
Fig. 7.   Alignment target image.

Fig. 9.   X-Y recorder output of alignment detection system.   Each trace was taken twice, and the target was moved 0.1 mm between traces 1 and 2.
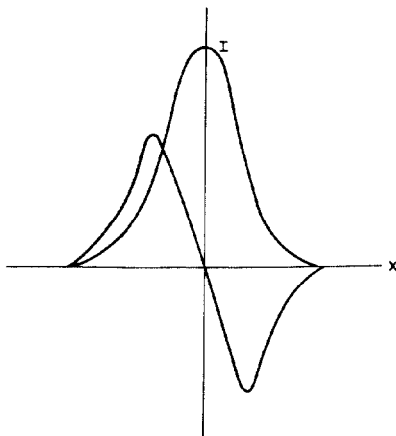
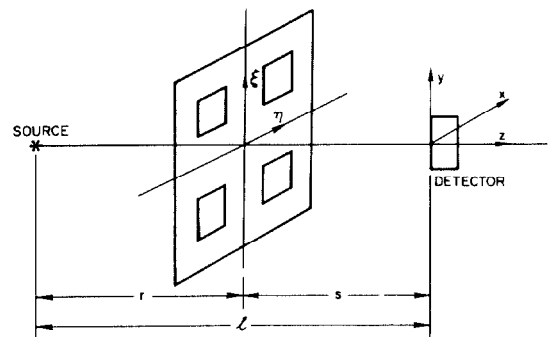Fig. 8.   Illustration of the relation between the intensity curve and the derivative curve.

Fig. 10.   Target coordinate system.